NASA Technical Memorandum 87598

Effect of Debond Growth on Stress-Intensity Factors in a Cracked Orthotropic Sheet Stiffened by a Semi-Infinite Orthotropic Sheet

C. A. Bigelow

JANUARY 1986

NASA

NASA Technical Memorandum 87598

Effect of Debond Growth on Stress-Intensity Factors in a Cracked Orthotropic Sheet Stiffened by a Semi-Infinite Orthotropic Sheet

C. A. Bigelow
Langley Research Center
Hampton, Virginia

National Aeronautics
and Space Administration

Scientific and Technical Information Branch

1986

Summary

Although stringers are used primarily as stiffeners, they also can make damaged structures fail-safe or damage tolerant. Assessment of the damage tolerance of structures weakened by cracks is aided by knowledge of stress-intensity factors. In this paper, the stress-intensity factors are determined for a cracked orthotropic sheet adhesively bonded to an orthotropic stringer where the adhesive layer is allowed to debond in accordance with an adhesive failure criterion. It is assumed that the debond penetration under the stringer is small compared with the width of the stringer. Based on this assumption, the stringer is modeled as a semi-infinite sheet bonded to an infinite sheet with a finite through-the-thickness crack in the infinite sheet. Modeling the adhesive layer with a nonlinear elastic stress-strain curve is also considered. Since the stringer is modeled as a semi-infinite sheet, the solution is most appropriate for a crack tip located near a stringer edge. Both the sheet and the stringer are treated as homogeneous, orthotropic media which are representative of many fiber-reinforced composite materials. It is assumed that the sheet and the stringer are in a state of plane stress and the adhesive is in pure shear. By using Green's functions and the complex variable theory of orthotropic elasticity developed by Lekhnitskii, a set of integral equations is obtained. The integral equations are replaced by an equivalent set of algebraic equations, which are solved to obtain the shear-stress distribution in the adhesive layer. Using these adhesive stresses, the crack-tip stress-intensity factors are found.

The effect of adhesive failure on the stress-intensity factors is examined. Debonding of the adhesive layer is found to cause an increase in the stress-intensity factors compared with the solution for an intact bond. The larger the debond area, the less effective the stringer is in reducing the stress-intensity factors. A debond area with a width and height greater than or equal to the half-crack length virtually eliminates the effect of the stringer.

To predict the debond areas, a rupture criterion based on the combined adhesive stresses is introduced. When the crack is not under the stringer, the majority of the debond growth is found to be along the edge of the stringer. When the crack tip is beneath the stringer, the debond first grows to the end of the crack; the majority of the subsequent growth is along the edge of the stringer. The stress level required to start debonding in the adhesive decreases as the crack tip is moved further beneath the stringer.

The effect of debonding and a nonlinear stress-strain curve for the adhesive are also examined. With the nonlinear adhesive, the debond initiates at higher applied stress levels than with the linear adhesive. The debond areas are slightly smaller than those found for the linear adhesive cases.

Debonding with the linear elastic adhesive causes the largest increase in the stress-intensity factors when compared with the intact bond case, where the larger the debond area, the greater the increase in the stress-intensity factors. Compared with the linear adhesive solution, modeling a nonlinear adhesive causes the stress-intensity factor to increase when the adhesive bond is assumed to remain intact, but causes the stress-intensity factor to decrease when debonding is included in the model.

Introduction

Fibrous composite materials are light, stiff, and strong; therefore, they have great potential for reducing weight in aircraft structures. In general, the structural configurations used in composite airplanes have been similar to the sheet-stringer construction currently used in metal airplanes. In metal airplanes, stringers are effective in making damaged structures fail-safe or damage tolerant. Because of this wide use, the interaction of a through-the-thickness crack and a stringer is an important problem and has been investigated by many authors.

A brief review of some of the work dealing with the problem of a stringer bonded to a sheet containing a crack begins with the 1959 investigation of Sanders (ref. 1), in which he treated the problem of a crack positioned symmetrically beneath a continuously attached stringer. He employed a shear-lag line stringer and assumed the sheet to be inextensible in the direction parallel to the crack to obtain the stringer stress-concentration factor and the crack-tip stress-intensity factor. In 1965, Greif and Sanders (ref. 2) removed Sanders' previous inextensionality assumption and symmetry requirements. They concluded that the stringer-induced reduction in the stress-intensity factor was a localized effect and that the stringer stress-concentration factor was largely insensitive to sheet stiffness in the direction parallel to the crack.

In 1974, Arin (ref. 3) examined the effect of a partially debonded, infinite stringer on the stress-intensity factor at the crack tip. He assumed that the stringer was adhesively bonded to an isotropic sheet along a line perpendicular to the crack, and he concluded that the stringer was ineffective unless it was quite close to the crack tip and the length of the debond was less than twice the crack length. However, since Arin was modeling the stringer as a

line, he was not able to account for partial debonding across the width of the stringer. Anderson, Hsu, and McGee (ref. 4) considered the growth of a crack initiating at a hole in an isotropic sheet reinforced by a bonded doubler in 1975. Their results, based on a two-dimensional finite-element analysis, indicated that the stress-intensity factor was unusually insensitive to crack length and that adhesive debond zones tended to follow the tip of the crack with little subsequent growth perpendicular to the crack line.

In 1978, Anderson, Chu, and McGee (ref. 5) assessed the growth characteristics of a fatigue crack approaching and growing beneath an adhesively bonded doubler. In this work, a two-dimensional finite-element analysis was used to compute the stress-intensity factor as a function of crack length for linear and nonlinear representations of the adhesive. The nonlinear representation of the adhesive predicted debonded areas that agreed extremely well with the experimentally observed debond in a bonded joint with aluminum adherends. The nonlinear representation of the adhesive was also found to reduce the stress-intensity factor relative to the solution for the linear elastic adhesive when debonding was included in both models of the adhesive layer.

In 1981, using a complex-variable approach, Norris (ref. 6) represented the finite-width stringer by an array of line stiffeners. The stringer was divided into strips, and each strip was modeled by a line stiffener attached to the sheet at discrete points with no coupling between adjacent line elements. This analysis did not model debond of the adhesive; thus, load predictions were unrealistically high in the line stiffener nearest the crack tip.

In reference 7, the solution to this problem assuming a linear elastic adhesive with an intact bond is presented. The parameter with the greatest influence on the stress-intensity factors was found to be the distance from the crack tip to the edge of the stringer. Unless the crack tip was very close to or under the stringer, the stress-intensity factor was approximately that of an unstiffened sheet. However, as the crack propagated beneath the stringer, the stress-intensity factor decreased significantly. Increasing the stringer stiffness or the adhesive stiffness also resulted in a decrease in the stress-intensity factor.

In reference 8, the solution to this problem assuming a nonlinear elastic adhesive with an intact bond is presented. When the adhesive was modeled with a nonlinear stress-strain curve, the peak stresses in the adhesive were considerably reduced in comparison to the solution for the linear elastic adhesive. This reduction resulted in increases in the stress-intensity factors due to the nonlinearity of the adhesive.

Experimental work has shown that as the crack tip approaches the stringer, debonding may start and propagate through the adhesive (ref. 5). Additionally, the adhesive may exhibit regions of nonlinear behavior. A need exists for an analysis that can be used to evaluate the effect of adhesive nonlinearity and a growing debond area on crack propagation in adhesively bonded structures. The purpose of the current work is to develop such an analysis and use it to predict the extent of stringer debonding and the effects of the debonding on the stress-intensity factors for cracks in a composite-material sheet/stringer configuration. Trends are developed for the effects of applied stress level, location of the crack tip relative to the stringer edge, and linear versus nonlinear adhesive behavior.

Nomenclature

a	half-length of crack, m
$+a$	right crack tip, m
$-a$	left crack tip, m
b	distance from edge of stringer to center of crack, m
D	domain of integration
d_x, d_y	constants in piecewise linear approximation of adhesive stress-strain curve
E_x, E_y	Young's moduli in x- and y-directions, respectively, Pa
f_{01}, f_{02}	stress functions, m^3/N
G_{xy}	orthotropic shear modulus, Pa
G_3	shear modulus of adhesive layer, Pa
h_j	thickness of layer j, m
k_1	mode-I component of stress-intensity factor, $Pa\sqrt{m}$
L/D	linear elastic adhesive with adhesive debonding
L/I	linear elastic adhesive with intact bond
N/D	nonlinear elastic adhesive with adhesive debonding
N/I	nonlinear elastic adhesive with intact bond
m_x, m_y	reciprocals of local slope in x- and y-directions, respectively, 1/Pa

N	number of cells or number of collocation points in domain
R_x, R_y	major and minor axes of debonded area, m
r_x, r_y	coordinate axes of debonded area, m
S_{jk}	complex kernels in integral equations ($j, k = 1, 2$), 1/(Pa-m)
W_1, W_2	complex kernels in stress-intensity-factor equations
X_j, Y_j	body forces acting on layer j ($j = 1, 2$), N/m^3
x, y	Cartesian coordinates, m
x_0, y_0	coordinates of concentrated load point, m
$\Delta x_j, \Delta y_j$	incremental distances ($j = 1, N$), m
γ	shear strain
ν_{xy}, ν_{yx}	Poisson's ratios
σ_0	crack-face pressure, Pa
τ	shear stress, Pa
τ_j, γ_j	arbitrary point on adhesive stress-strain curve
τ_R	rupture strength of adhesive in shear, Pa
τ_x, τ_y	adhesive shear stresses, Pa

Analytical Procedures

Formulation of Problem

Consider the configuration shown in figure 1. It is assumed that the debond penetration under the stringer is small compared with the width of the stringer. Based on this assumption, the stringer is modeled as a semi-infinite sheet bonded to an infinite sheet with a finite, through-the-thickness crack in the infinite sheet. Hereinafter, the semi-infinite sheet is referred to as a stringer. The stringer and the infinite sheet are bonded together by an adhesive layer of constant thickness h_3. It is assumed that the adherends are in a state of plane stress and the adhesive is in pure shear. Both the infinite sheet and the stringer are made of a fiber-reinforced plastic which is treated as a homogeneous, orthotropic, linearly elastic medium. The model is loaded by a uniform pressure σ_0 on the crack faces with the stress state at infinity equal to zero, as shown in figure 1. As explained in the appendix, the present solution for the uniformly stressed crack face is a close approximation for the corresponding problem with a remote applied stress.

Integral Equations for Adhesive Shear Stresses

By using Green's functions and the complex variable theory of orthotropic elasticity developed by Lekhnitskii, a set of integral equations describing the problem was formulated (refs. 7, 8, and 9). For elastic nonlinear adhesive behavior, the problem in figure 1 was reduced to the solution of the integral equations which follow.

$$\left.\begin{aligned} h_3 m_x \tau_x(x,y) + \iint_D \left[S_{11}(x,y,x_0,y_0)\,\tau_x(x_0,y_0)\right. \\ \left. + S_{12}(x,y,x_0,y_0)\,\tau_y(x_0,y_0)\right] dx_0\, dy_0 \\ = \sigma_0 f_{01}(x,y) - h_3 d_x \\ h_3 m_y \tau_y(x,y) + \iint_D \left[S_{21}(x,y,x_0,y_0)\,\tau_x(x_0,y_0)\right. \\ \left. + S_{22}(x,y,x_0,y_0)\,\tau_y(x_0,y_0)\right] dx_0\, dy_0 \\ = \sigma_0 f_{02}(x,y) - h_3 d_y \end{aligned}\right\} \quad (1)$$

Here τ_x and τ_y are the unknown adhesive shear stresses in the x- and y-directions, respectively, and the kernels S_{jk} ($j, k = 1, 2$) and the functions f_{01} and f_{02} are known; m_x and m_y are the reciprocals of the local slope of the adhesive shear stress-strain curve, and d_x and d_y are constant terms in the piecewise linear approximation of the adhesive stress-strain curve; D is the region of the adhesive bond. (The appendix details the derivation of equations (1).) For the linear adhesive case, equations (1) are simplified as follows:

$$m_x = m_y = 1/G_3$$

$$d_x = d_y = 0$$

The solution of equations (1) produces the shear-stress distribution in the adhesive τ_x and τ_y. For the linear elastic representation of the adhesive, these equations need only be solved once. When the nonlinear stress-strain curve is used to model the adhesive, these equations are solved iteratively using a piecewise linear approximation of the adhesive stress-strain curve. Once the adhesive stresses are known, the stress-intensity factor at either crack tip can be found, and the debond area can be predicted.

Numerical Solution of Integral Equations

Because of the complicated nature of equations (1), a closed-form integration is difficult if not impossible to perform. Since the kernels $S_{jk}\,(j,k=1,2)$ contain only logarithmic singularities and are integrable in the infinite domain D, equations (1) can be treated as Fredholm equations of the second kind. Consequently, the system of equations can be solved with standard numerical techniques. This is done by dividing the domain into small cells, assuming the unknown functions τ_x and τ_y to be uniform in each cell, and then using a numerical scheme to evaluate the equations.

When the integrals in equations (1) are replaced by summations, the following system of equations is obtained:

$$\left.\begin{aligned} &h_3 m_x \tau_x(x_j,y_j) + \sum_{n=1}^{N}\left[S_{11}(x_j,y_j,x_{0_n},y_{0_n})\right.\\ &\quad\times\tau_x(x_{0_n},y_{0_n}) + S_{12}(x_j,y_j,x_{0_n},y_{0_n})\\ &\quad\left.\times\,\tau_y(x_{0_n},y_{0_n})\right]\Delta x_n\Delta y_n\\ &\quad= \sigma_0 f_{01}(x_j,y_j) - h_3 d_x \quad (j=1,N)\\ &h_3 m_y \tau_y(x_j,y_j) + \sum_{n=1}^{N}\left[S_{21}(x_j,y_j,x_{0_n},y_{0_n})\right.\\ &\quad\times\tau_x(x_{0_n},y_{0_n}) + S_{22}(x_j,y_j,x_{0_n},y_{0_n})\\ &\quad\left.\times\,\tau_y(x_{0_n},y_{0_n})\right]\Delta x_n\Delta y_n\\ &\quad= \sigma_0 f_{02}(x_j,y_j) - h_3 d_y \quad (j=1,N) \end{aligned}\right\} \quad (2)$$

where N is the number of collocation points or the number of cells in the domain.

The outer boundary of the domain D theoretically goes to infinity. However, to carry out the numerical analysis, the size of D must be restricted. A convergence study was conducted to determine the extent and refinement necessary so that the critical quantities of interest, the stress-intensity factors, were not appreciably affected by the restriction. Thus, for the linear elastic adhesive solution (ref. 7), the size of D was determined iteratively, starting with a small, coarse mesh and increasing the extent and refinement until no significant changes occurred in the stress-intensity factor. In reference 8, it was determined that the same mesh could be used with the nonlinear adhesive equations as was used with the linear adhesive. A typical mesh layout used in the analysis is shown in figure 2, where, because of the symmetry, only one-half of the integration domain is shown.

Determination of Stress-Intensity Factors

In the present problem, because of symmetries in the geometry and loading, the shear component of the stress-intensity factor is zero. The normal component is found by combining the effects of the crack-face pressure σ_0 and the adhesive shear forces τ_x and τ_y acting on the infinite sheet. The stress-intensity factor may be expressed in terms of the unknown shear forces as follows:

$$k_1(a_0) = \sigma_0\sqrt{a} + \frac{2a_0}{a\sqrt{a}h_1}\iint_D \left[W_1(x,y,x_0,y_0)\,\tau_x(x_0,y_0)\right.$$
$$\left. + W_2(x,y,x_0,y_0)\,\tau_y(x_0,y_0)\right]dx_0dy_0 \quad (3)$$

where a_o is replaced by $+a$ for the right crack tip and by $-a$ for the left crack tip. The terms W_1 and W_2 are functions of the crack length, edge distance of the stringer, and the material properties of the infinite sheet. Complete details on the derivation of the equation for the stress-intensity factors are given in reference 7.

Prediction of Debonding

To predict the boundary of the debond area, a simple rupture criterion based on the adhesive shear stresses is introduced. This criterion, shown in equation (4), states that within the debond area, the state of combined shear stress in the adhesive is greater than or equal to τ_R, the rupture strength of the adhesive in shear, where τ_R is known. The adhesive failure criterion is written as follows:

$$\sqrt{\left[\tau_x^2(x,y) + \tau_y^2(x,y)\right]} \geq \tau_R \quad (4)$$

This failure criterion is based on the octahedral shearing-stress theory (also referred to as the Mises-Hencky, or simply the Von Mises, criterion) where the ultimate shear strength of the adhesive τ_R has replaced the yield strength found in the Von Mises equation. Since the only stresses assumed to be present in the adhesive layer are the shear stresses, only these terms appear in the failure criterion.

Linear adhesive. To determine the boundary of the debond area for the linear adhesive, the adhesive shear stresses in each cell are first found assuming no debond. At the given applied stress, every cell where equation (4) is true is assumed to be debonded. Using this new debond area, the adhesive shear stresses are determined again and compared with equation (4) to find any additional debonding. If there is any, the new debond area is used to recalculate the adhesive stresses. This iteration process

continues until there is no new debond area at the current level of applied stress. For each consecutive level of applied stress, the debond area determined from the previous level is used to start the iteration.

Nonlinear adhesive. The debond area for the nonlinear adhesive is found in a similar manner. First, the adhesive shear stresses are found assuming no debonding of the adhesive layer. In this case, though, equations (2) must be solved iteratively. Then, as with the linear adhesive, every cell where equation (4) is true is assumed to be debonded; the procedure follows as in the linear adhesive case, where equations (2) are solved iteratively for each new assumed debond area.

Results

For the results presented, the infinite sheet (layer 1) is modeled as a quasi-isotropic graphite/epoxy laminate and the stringer (layer 2) as a unidirectional graphite/epoxy laminate. The material properties (ref. 10) are given in table I. For the elastic linear adhesive, a shear modulus of 560 MPa was used. The rupture strength of the adhesive in shear τ_R is taken as 37.9 MPa. These values are typical of the AF-127 adhesive (ref. 5). The adhesive stress-strain curves used to model the adhesive behavior are shown in figure 3. The thickness of the base sheet h_1 is 2.0 mm, the thickness of the stringer h_2 is 1.0 mm, and the adhesive thickness h_3 is 0.01 mm.

Effect of Stringer Debond Size and Shape on Stress-Intensity Factors

The effect of adhesive debonding on the stress-intensity factors k_1 is investigated by assuming various debond sizes and shapes. Figure 4 shows the configuration of the assumed debond; R_x and R_y are the half-lengths along the axes of the elliptical debond area in the x- and y-directions, respectively. The values of R_x and R_y are varied to produce different debond sizes. A value of zero for either R_x or R_y indicates no debonding of the adhesive (i.e., a zero debond area). Although the crack as shown in figure 4 is not beneath the stringer, for most of the results presented, the crack is partially beneath the stringer. In the following figures, only results for the crack tip nearest the stringer are shown, because the size of the debond area has almost no effect on the stress-intensity factors for the crack tip farthest from the stringer.

Figure 5 shows a series of curves in which the value of R_x is varied and R_y is held constant for $a/b = 5.0$. The location of the crack tip in relation to the edge of the stringer is noted in the figure. For all the values of R_y considered, the results show that the stringer must be debonded nearly to the end of the crack before the value of k_1 begins to increase. Once the debond is extended past the crack tip, the maximum increase in k_1 is quickly obtained, and further debond growth has little effect on k_1. For increasing values of R_y, the height of the debond, the limiting value approaches 1.0, the solution for the unstiffened sheet, as expected.

In figure 6, the value of R_y is varied while R_x is held constant for $a/b = 2.0$. The debond width was chosen so that $a/R_x = a/b = 2.0$; this locates the end of the debond area at the crack tip. As indicated in figure 6, in this example two debond shapes are considered: a rectangular area and an elliptic area. The change in the crack-tip stress-intensity factor as the debond areas increase is shown in the figure. The rectangular debond results in larger increases in k_1 than does the elliptic debond. This is expected, since, for the same values of R_x and R_y, a rectangle has more area than an ellipse. Thus, with the larger debond area, the stringer is less effective in reducing k_1. However, as the value of R_y increases (i.e., as the debond grows along the edge of the stringer), differences between a rectangular debond and an elliptic debond decrease. As R_y approaches infinity, the solution for k_1 should approach the solution for $b = a$, as indicated in figure 6.

Figure 7 shows the effect of assuming that the debond has extended completely across the width of the stringer (i.e., $R_x = \infty$). The stress-intensity factor is plotted at various levels of R_y for increasing values of a/b. For values of a/b less than 1.0, the debond height has little effect on the crack-tip stress-intensity factor. However, for $a/b > 1.0$, that is, when the crack tip is beneath the stringer, the effect of the stringer is progressively reduced as R_y becomes larger. As R_y becomes very large, the values of k_1 approach those of the unstiffened sheet.

Predicted Stringer Debonding

Linear adhesive. Figures 8, 9, and 10 show the predicted debond areas at increasing levels of applied stress for $a/b = 0.95$, 1.05, and 2.0, respectively. These values of a/b were chosen to illustrate three particular cases of interest: (1) the crack tip close to but not under the stringer; (2) the crack tip a small distance beneath the stringer; and (3) the crack tip a large distance beneath the stringer.

For $a/b = 0.95$ (fig. 8), the right crack tip is located slightly beneath the edge of the stringer. In this case, debonding does not start until the applied stress reaches 70 MPa. With increasing applied stress

level, the debond grows significantly along the edge of the stringer but very little under the stringer.

Figure 9 shows the predicted debond growth for $a/b = 1.05$. In this case, the crack tip is beneath the stringer, slightly past the edge of the stringer. The debonding begins at a much lower stress level for this case than for $a/b = 0.95$. For $a/b = 1.05$, the debond initiates at an applied stress of 15 MPa. Once the debond is initiated at the stringer edge, it grows first to the crack tip, and then the rest of the debond growth is primarily along the stringer edge.

When the crack tip is far beneath the stringer ($a/b = 2.0$), as shown in figure 10, the debonding starts at an even lower applied stress than with the two previous cases. Here, the debond initiates at an applied stress of 7.5 MPa and grows diagonally until the debond reaches the crack tip. Once the debond reaches the crack tip, it continues to extend parallel to the edge of the stringer, as in the previous cases.

Nonlinear adhesive. Using the stress-strain curve shown in figure 3, the debond growth for the nonlinear adhesive is predicted for $a/b = 0.95$, 1.05, and 2.0. For the materials considered, the solution of the nonlinear equations typically required 8 to 10 iterations for convergence.

Figure 11 shows the predicted debond area for $a/b = 0.95$, assuming a nonlinear elastic adhesive. The debond initiates at an applied stress of 150 MPa, which is much higher than the stress level required for debond initiation in the linear elastic adhesive case. Also, the debond does not start at $y = 0$ (the crack plane), as in the linear adhesive case, but starts at the edge of the stringer some distance above the crack. Additionally, compared with the linear adhesive case, equal increments of stress produce less debond growth for the nonlinear adhesive.

Figure 12 shows the predicted debond area for $a/b = 1.05$, assuming a nonlinear elastic adhesive layer. The debond initiates at an applied stress of 30 MPa, compared with a stress of 15 MPa required to initiate the debond for the linear adhesive case. Comparison of figures 9 and 12 shows that the debond trends are similar for the linear and nonlinear adhesive models but that higher stresses are required to grow the debond for the nonlinear adhesive.

Figure 13 shows the predicted debond area for the nonlinear adhesive for $a/b = 2.0$. Here, the debond initiates at an applied stress of 15 MPa, compared with 7.5 MPa required for debond initiation in the linear adhesive case. Again, comparison of figures 10 and 13 shows that the debond does not grow as readily with the nonlinear adhesive as with the linear adhesive, although the trends are similar.

Predicted Stress-Intensity Factors

Figures 14 and 15 compare the normalized stress-intensity factors for four conditions: linear elastic adhesive with an intact bond (L/I), linear elastic adhesive including debonding (L/D), nonlinear elastic adhesive with an intact bond (N/I), and nonlinear elastic adhesive including debonding (N/D). Figure 14 shows the normalized k_1 for $a/b = 1.05$, and figure 15 shows k_1 for $a/b = 2.0$, at both the left, $k_1(-a)$, and right, $k_1(+a)$, crack tips for increasing levels of applied stress. For the intact conditions, in most cases, the applied stress levels used in these figures produce adhesive stresses greater than τ_R, the adhesive rupture strength. However, for the intact cases, the adhesive was assumed not to rupture to allow for comparisons with the debond cases. Thus, for these data points, the adhesive stress-strain curves shown in figure 3 were extended past the point of adhesive failure in a straight line having the same slope as the final portion of the curves.

As shown in figures 14 and 15, modeling adhesive debonding, nonlinearity, or the combination of the two, causes k_1 to increase compared with the linear intact case. For all conditions, except the linear intact case, normalized k_1 increases with increasing level of applied stress. The effect of adhesive debonding and nonlinearity on the stress-intensity factors at the left crack tip is much less than at the right crack tip.

Figures 14 and 15 show that, for the conditions examined, debonding of the linear adhesive produces the largest increase in k_1. Also, the greater the applied stress, the larger the increase in k_1. This is particularly evident for $a/b = 2.0$ (fig. 15). In this case, for an applied stress of 25 MPa, the debonding of the linear adhesive is so extensive that the effect of the stringer in reducing k_1 is almost entirely eliminated.

An interesting comparison can be made for the nonlinear adhesive with the intact and debond conditions from figures 14 and 15. (The data shown in figures 14 and 15 are listed in table II.) Including the nonlinearity of the adhesive with the intact bond condition causes the stress-intensity factors to increase relative to the linear intact condition. However, including the nonlinearity of the adhesive with the debond condition causes the stress-intensity factors to decrease relative to the linear debond condition. This agrees with the conclusion reached in reference 5, which was that modeling a nonlinear adhesive causes the stress-intensity factor to decrease. (The analysis of ref. 5 included debonding of the adhesive in the model.) This also supports the conclusion of references 8 and 11, which showed that

modeling a nonlinear adhesive results in increases in the stress-intensity factors. (Neither refs. 8 nor 11 considered debonding of the adhesive layer.)

Conclusions

This report presents the formulation of an analysis for a cracked orthotropic sheet reinforced with an adhesively bonded orthotropic semi-infinite sheet. This configuration was assumed to represent a bonded stringer panel when the crack is located close to the edge of the stringer, and any debonding of the adhesive layer is small compared with the width of the stringer. The effect of debond growth and adhesive nonlinearity on the crack-tip stress-intensity factors was examined using the analysis. Based on this study, the following conclusions were drawn:

1. For the linear elastic adhesive, debonding of the stringer near the crack caused the stress-intensity factors to increase relative to the intact bond condition, and, when the debond dimensions exceeded the crack half-length, the stress-intensity factors approached those of the unstiffened sheet.
2. When the adhesive was modeled as a linear elastic material, the analysis indicated that (a) when the crack is not beneath the stringer, the majority of the debond growth is along the edge of the stringer; (b) when the crack tip is beneath the stringer, the debond first grows to the crack tip and then along the edge of the stringer; and (c) the stress level required to start the debond growth in the adhesive layer decreases as the crack tip moves towards and beneath the stringer.
3. When adhesive nonlinearity is modeled in the analysis, the applied stress levels required to initiate debonding increase significantly compared with the stress levels required for the linear elastic adhesive, and the predicted debond does not extend as readily as for the linear adhesive.
4. For both the linear and nonlinear representations of the adhesive layer, the stress-intensity factors increased when debonding was allowed to occur according to the assumed adhesive failure criterion. Including debonding with the linear elastic adhesive caused the stress-intensity factors to increase relative to the linear intact condition, but including debonding with the nonlinear adhesive caused the stress-intensity factors to decrease relative to the nonlinear-intact condition. That is, when debonding was included, the stringer was more effective with the nonlinear adhesive.

NASA Langley Research Center
Hampton, VA 23665-5225
October 9, 1985

Appendix

Formulation of Integral Equations for Bonded System

This appendix is a brief summary of the formulation of the integral equations for the solution to the problem of the semi-infinite orthotropic sheet bonded to a cracked orthotropic sheet. The complete details of this formulation can be found in references 7 and 9.

Consider the stringer configuration shown in figure 1. (Hereinafter, the semi-infinite sheet will be referred to as a stringer.) The stringer and the sheet are bonded together by an adhesive layer of constant thickness h_3.

The model is loaded by a uniform pressure σ_0 on the crack faces with the stress state at infinity equal to zero as shown in figure A1. If the two layers have equal minor in-plane Poisson's ratios ν_{yx}, the stress-intensity-factor solution formulated here for the uniformly stressed crack face is identical to the problem of the remotely loaded stringer panel. On the other hand, if $\nu_{yx}^{(1)} \neq \nu_{yx}^{(2)}$, as is the case here, the displacements in the x-direction will differ for the two loading cases. Therefore, the two solutions will not be equivalent. However, it is shown in reference 9 that the differences in the two solutions are not large. For the graphite-epoxy laminates considered, the error introduced by this approximation is less than 5 percent. Thus, the present solution for a uniformly stressed crack face is a close approximation to the solution for the corresponding case with remote loading.

For the problem shown in figure A1, the integral equations are formulated with the following assumptions:

1. The sheet (layer 1) and the stringer (layer 2) are homogeneous and linearly elastic; the adhesive (layer 3) is homogeneous, isotropic, and nonlinearly elastic.

2. The sheet and the stringer are dissimilar, orthotropic materials with principal directions of orthotropy being oriented parallel and perpendicular to the crack in layer 1.

3. The thickness of the sheet h_1 and the thickness of the stringer h_2 are small compared with the in-plane dimensions, so that both layers are considered to be in a state of plane stress.

4. The surface shear transmitted through the adhesive is assumed to act as a body force on the infinite sheet and the stringer.

5. The thickness of the adhesive h_3 is small compared with the thicknesses of the sheet and stringer; thus, the adhesive layer is treated as a shear spring rather than as an elastic continuum.

Assumption 5 leads to the following continuity of displacement equations:

$$u_1 - u_2 = \frac{h_3}{G_3}\tau_x \qquad v_1 - v_2 = \frac{h_3}{G_3}\tau_y \tag{A1}$$

where u_1, v_1 and u_2, v_2 are the x- and y-components of the in-plane displacement vectors in layers 1 and 2, τ_x and τ_y are the components of the adhesive shear stress, and h_3 and G_3 are the adhesive thickness and shear modulus, respectively. From assumption 3, the two sets of body forces (force per unit volume) that act on layers 1 and 2 (see fig. A1) can be written as follows:

$$X_1 = -\frac{\tau_x}{h_1} \qquad Y_1 = -\frac{\tau_y}{h_1} \qquad X_2 = \frac{\tau_x}{h_2} \qquad Y_2 = \frac{\tau_y}{h_2} \tag{A2}$$

Figure A1 shows how the problem is broken into its component parts. The displacements in the sheet, shown in part B of figure A1, and in the stringer, shown in part C of figure A1, are determined individually. The complete expressions for these displacements are given in reference 7. Equations (A2) are used to relate the forces X_1, Y_1, X_2, Y_2 to the adhesive shear stresses τ_x, τ_y. The displacements for each layer are substituted into equations (A1). Then, following the procedure used in reference 11, a relationship between the adhesive shear stress and strain is obtained by linear interpolation. If τ is the unknown stress on the stress-strain curve (fig. A2) and τ_{j-1} and τ_j are the adjacent points given on the stress-strain curve, where the corresponding shear strains are $\gamma_{j-1} \leq \gamma \leq \gamma_j$, then the relationship between γ and τ can be written as follows:

$$\gamma = \gamma_{j-1} + (\tau - \tau_{j-1})\frac{\gamma_j - \gamma_{j-1}}{\tau_j - \tau_{j-1}}$$

$$\gamma = m\tau + d$$

where

$$m = \frac{\gamma_j - \gamma_{j-1}}{\tau_j - \tau_{j-1}}$$

$$d = \gamma_{j-1} - m\tau_{j-1}$$

and

$$\gamma = \tau / G_3$$

Thus, for the nonlinear elastic adhesive, the problem reduces to the solution of the following integral equations:

$$\left.\begin{aligned} h_3 m_x \tau_x(x,y) + \iint_D [S_{11}(x,y,x_0,y_0)\,\tau_x(x_0,y_0) \\ + S_{12}(x,y,x_0,y_0)\,\tau_y(x_0,y_0)]\,dx_0\,dy_0 \\ = \sigma_0 f_{01}(x,y) - h_3 d_x \\ h_3 m_y \tau_y(x,y) + \iint_D [S_{21}(x,y,x_0,y_0)\,\tau_x(x_0,y_0) \\ + S_{22}(x,y,x_0,y_0)\,\tau_y(x_0,y_0)]\,dx_0\,dy_0 \\ = \sigma_0 f_{02}(x,y) - h_3 d_y \end{aligned}\right\} \quad \text{(A3)}$$

where D is the bonded region, and where the kernels $S_{jk}\,(j,k = 1,2)$ and the functions f_{01} and f_{02} are known. (See ref. 7 for details.) The kernels S_{jk} are related to the distributed body force loadings shown in parts B and C of figure A1 and are functions of the material properties of each layer, the half-crack length a, and the stringer edge distance b. The functions f_{01} and f_{02} are related to the uniform crack-face pressure σ_0 shown in part B of figure A1 and are functions of the material properties of layer 1 and the half-length of the crack a. The terms m_x and m_y represent the reciprocal slopes of the adhesive stress-strain curve (defined previously) in the x- and y-directions, respectively, and d_x and d_y are constant terms (defined previously) in the piecewise linear approximation of the adhesive stress-strain curve. Complete details on the derivation of these equations can be found in reference 8 or 9.

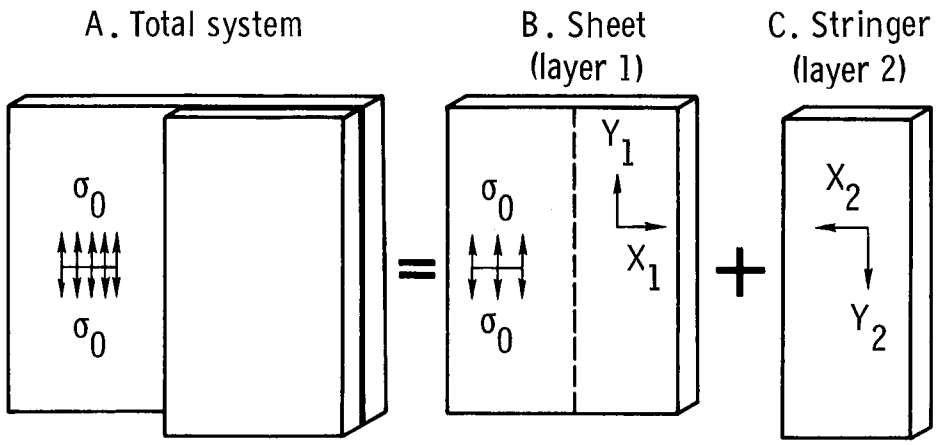

Figure A1. Superposition model of problem.

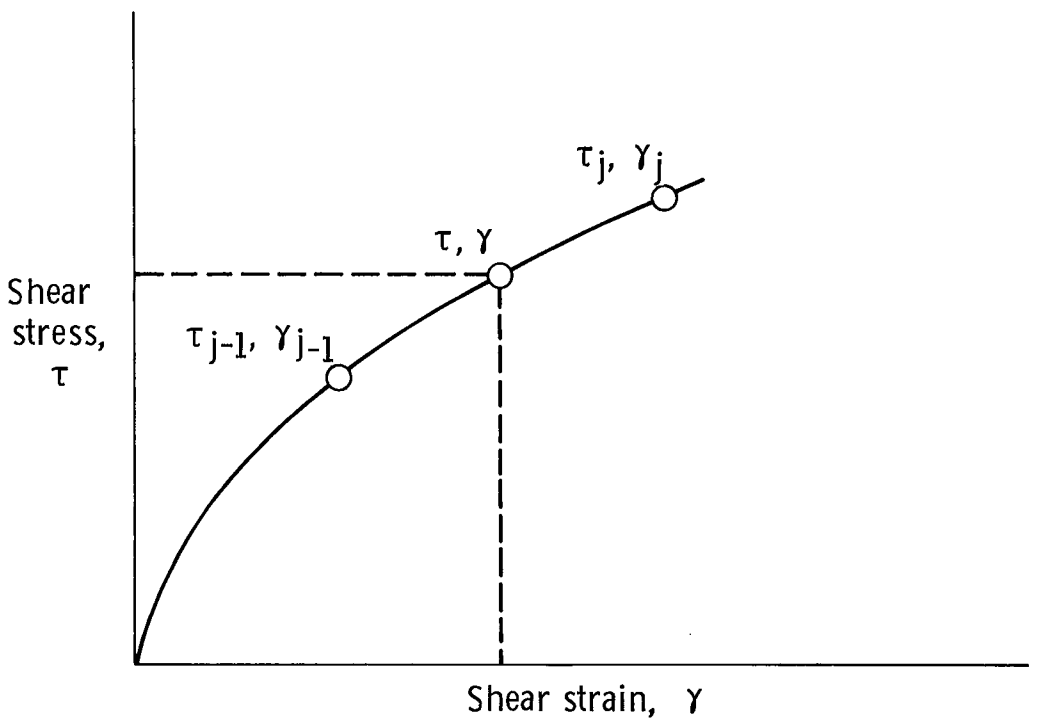

Figure A2. Schematic stress-strain curve of adhesive.

References

1. Sanders, J. Lyell, Jr.: *Effect of a Stringer on the Stress Concentration Due to a Crack in a Thin Sheet.* NASA TR R-13, 1959. (Supersedes NACA TN 4207.)
2. Greif, Robert; and Sanders, J. L., Jr.: The Effect of a Stringer on the Stress in a Cracked Sheet. Trans. ASME, Ser. E: *J. Appl. Mech.*, vol. 32, no. 1, Mar. 1965, pp. 59–66.
3. Arin, K.: A Plate With a Crack, Stiffened by a Partially Debonded Stringer. *Eng. Fract. Mech.*, vol. 6, no. 1, Mar. 1974, pp. 133–140.
4. Anderson, Jerry M.; Hsu, Teh Min; and McGee, Wade M.: Characterization of Crack Growth in Bonded Structures. *Proceedings 12th Annual Meeting of the Society of Engineering Science,* 1975, pp. 1283–1292.
5. Anderson, J. M.; Chu, C. S.; and McGee, W. M.: Growth Characteristics of a Fatigue Crack Approaching and Growing Beneath an Adhesively Bonded Doubler. *J. Eng. Mater. & Technol.*, vol. 100, no. 1, Jan. 1978, pp. 52–56.
6. Norris, M.: The Use of Bonded Crack-Stoppers in Pressure Cabins. *Aeronaut. J.*, vol. 85, no. 841, Feb. 1981, pp. 57–62.
7. Bigelow, C. A.: *A Cracked Orthotropic Sheet Stiffened by a Semi-Infinite Orthotropic Sheet.* NASA TP-2455, 1985.
8. Bigelow, C. A.: *Nonlinear Adhesive Behavior Effects in a Cracked Orthotropic Sheet Stiffened by a Semi-Infinite Orthotropic Sheet.* NASA TM-87584, 1985.
9. Bigelow, Catherine Ann: The Effect of Debond Growth on Crack Propagation in Composite Plates Reinforced With Adhesively Bonded Composite Stringers. Ph.D. Thesis, Georgia Inst. of Technol., Dec. 1984.
10. Poe, C. C., Jr.: *A Single Fracture Toughness Parameter for Fibrous Composite Laminates.* NASA TM-81911, 1981.
11. Kan, H. P.; and Ratwani, M. M.: Nonlinear Adhesive Behavior Effects in Cracked Metal-to-Composite Bonded Structures. *J. Eng. Fract. Mech.*, vol. 15, no. 1–2, 1981, pp. 123–130.

TABLE I. MATERIAL PROPERTIES

Layer	E_x, GPa	E_y, GPa	ν_{xy}	G_{xy}, GPa	τ_R, MPa	Material system
1	51.40	51.40	0.30650	19.67		$[0/\pm 45/90]_s$ graphite-epoxy
2	10.86	129.40	.02617	5.70		[0] graphite-epoxy
3				.56	37.9	AF-127 adhesive

TABLE II. PREDICTED STRESS-INTENSITY FACTORS

a/b	σ_0, MPa	Normalized stress-intensity factor at crack tip nearest stringer[1] for –			
		L/I	L/D	N/I	N/D
1.05	30.0	0.6679	0.7928	0.7214	0.7366
	40.0	.6679	.8250	.7383	.7725
	50.0	.6679	.8552	.7522	.7872
2.00	15.0	0.2081	0.2214	0.2105	0.2111
	20.0	.2081	.2908	.2142	.2165
	25.0	.2081	.9163	.2191	.2245
a/b	σ_0, MPa	Normalized stress-intensity factor at crack tip away from stringer[2] for –			
		L/I	L/D	N/I	N/D
1.05	30.0	0.9674	0.9690	0.9681	0.9683
	40.0	.9674	.9697	.9683	.9687
	50.0	.9674	.9707	.9685	.9690
2.00	15.0	0.8590	0.8797	0.8620	0.8635
	20.0	.8590	.8958	.8637	.8685
	25.0	.8590	.9965	.8654	.8739

[1] $\frac{k_1(+a)}{\sigma_0\sqrt{a}}$.

[2] $\frac{k_1(-a)}{\sigma_0\sqrt{a}}$.

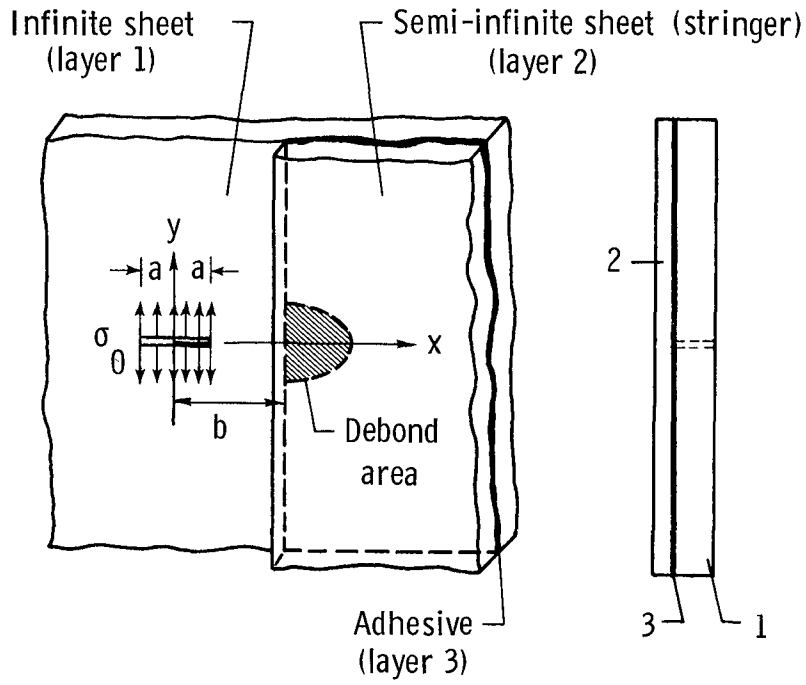

Figure 1. Configuration considered in problem.

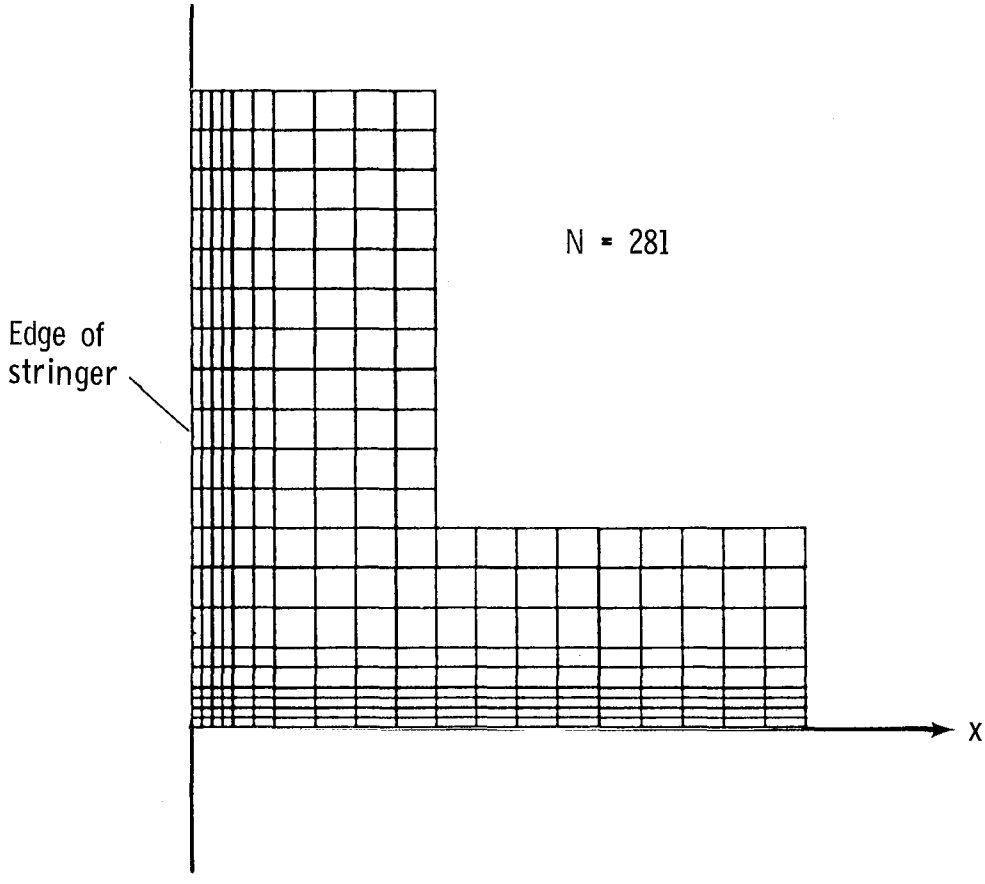

Figure 2. Typical mesh used in integration.

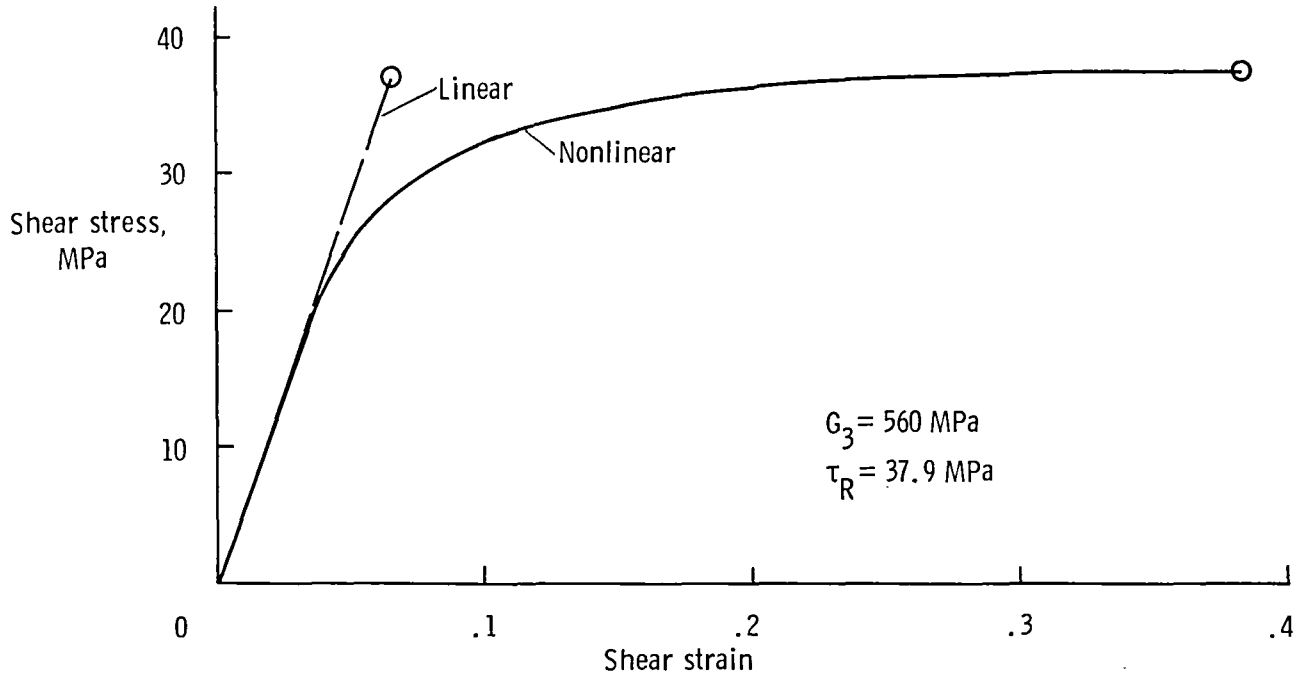

Figure 3. Shear stress-strain curve for AF-127 adhesive (ref. 5).

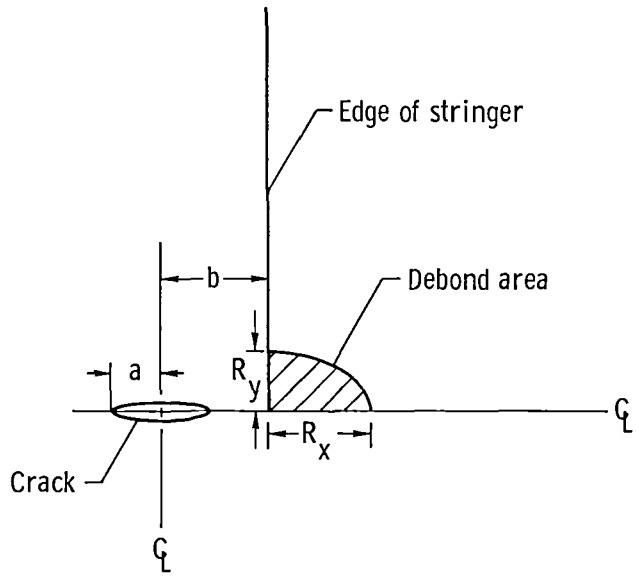

Figure 4. Configuration of debond area.

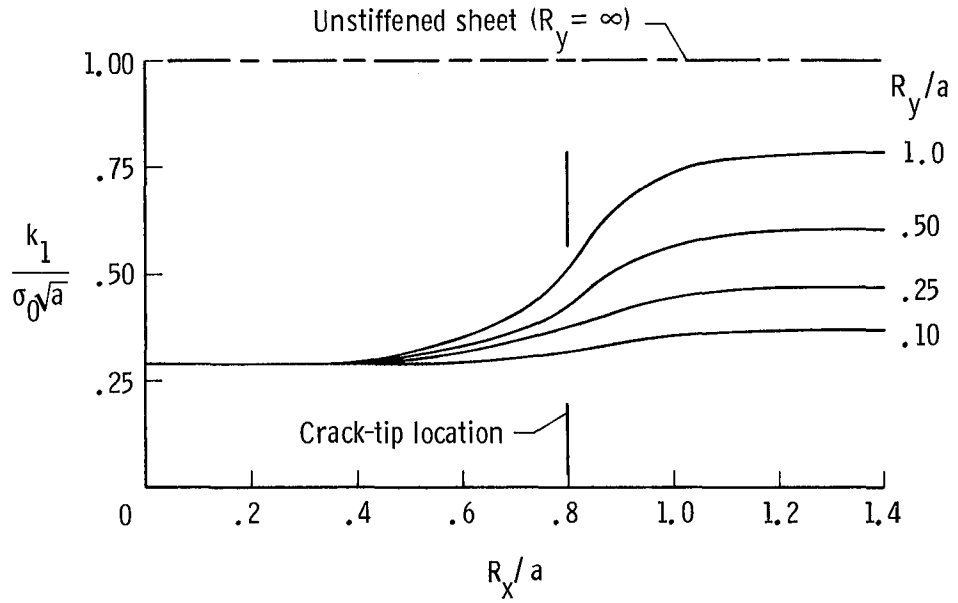

Figure 5. Normalized stress-intensity factor as a function of debond width and height. $a/b = 5.0$.

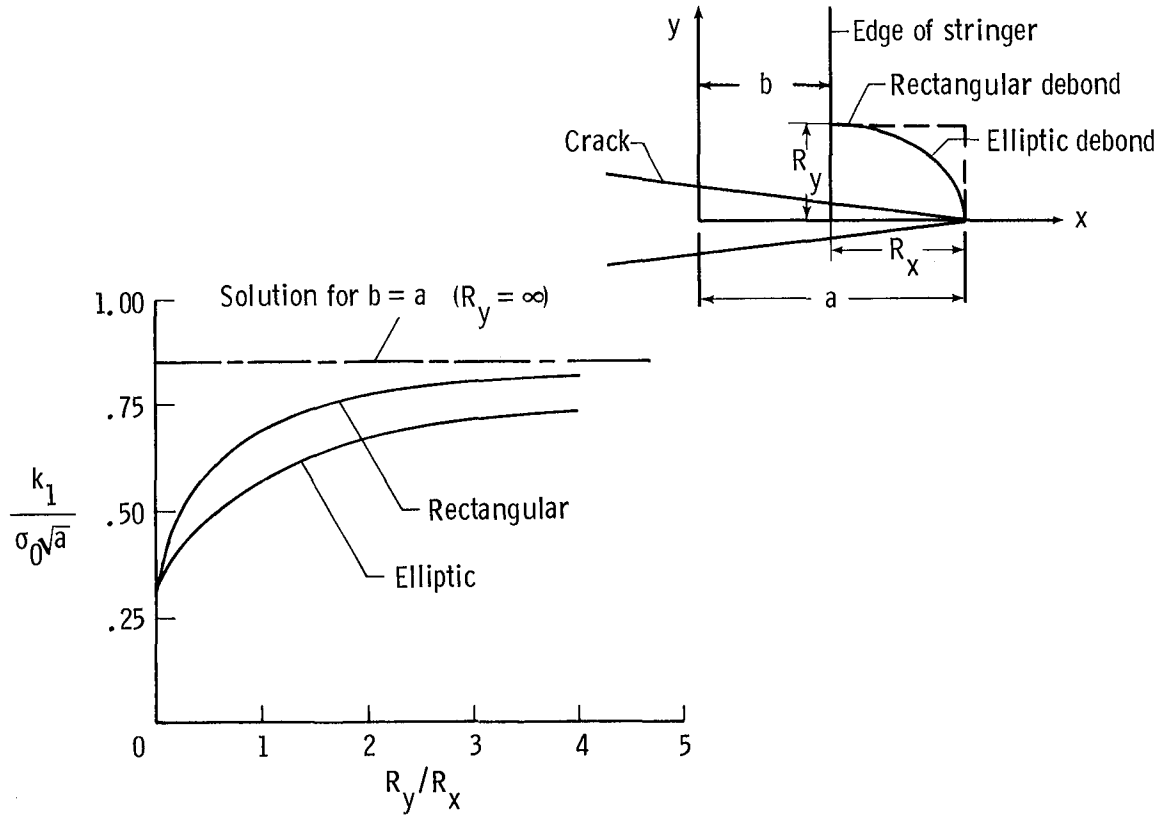

Figure 6. Normalized stress-intensity factor as a function of debond aspect ratio. $a/b = 2.0; a/R_x = 2.0$.

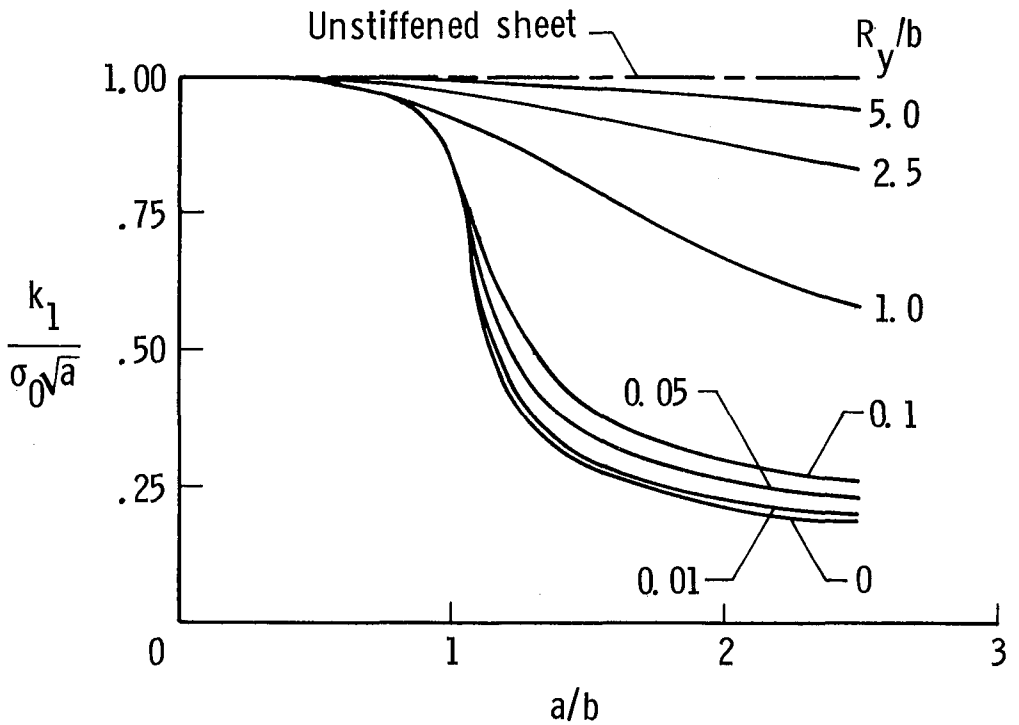

Figure 7. Normalized stress-intensity factor as a function of crack length and debond height. $R_x = \infty$.

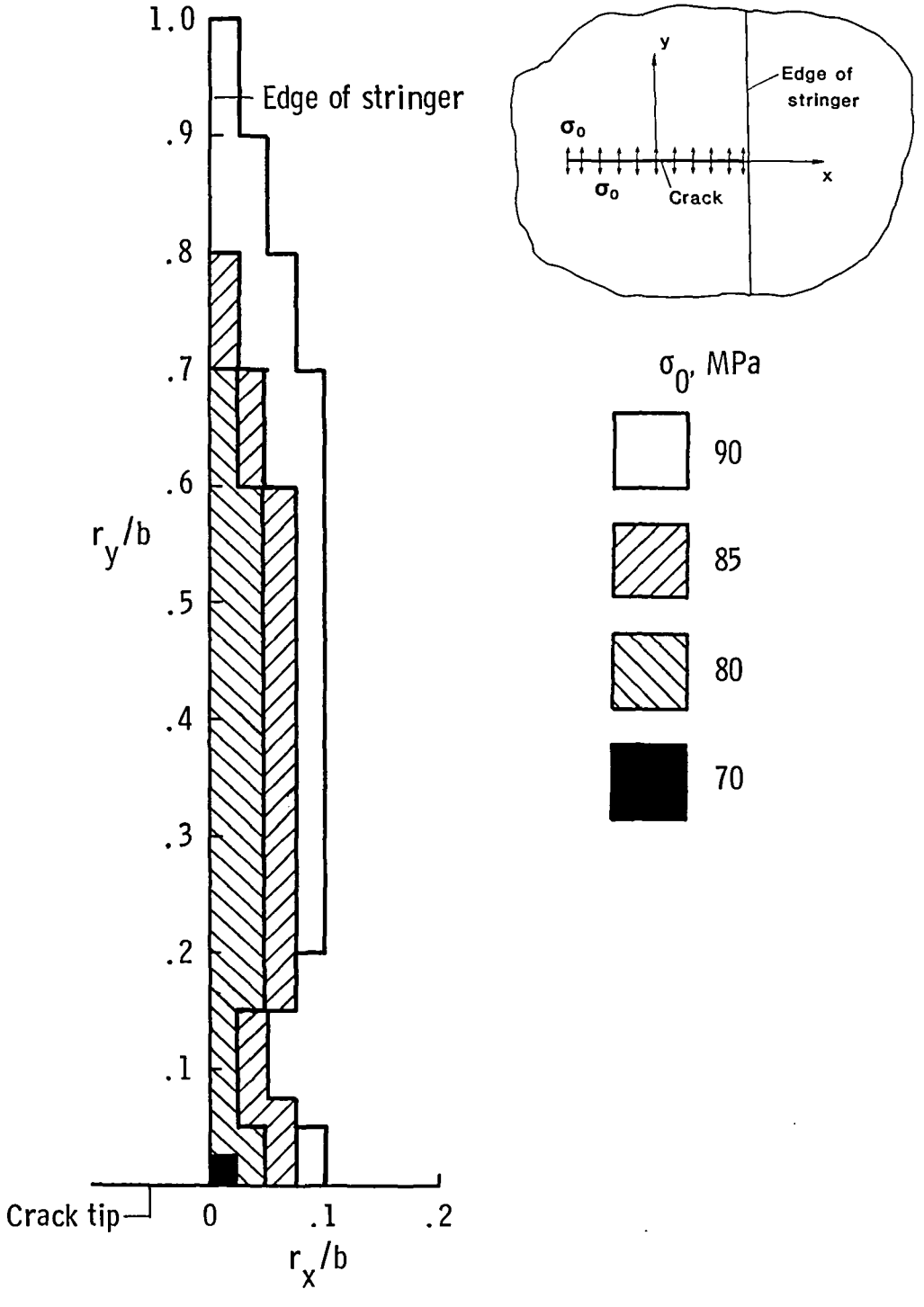

Figure 8. Predicted debond growth in linear adhesive for $a/b = 0.95$.

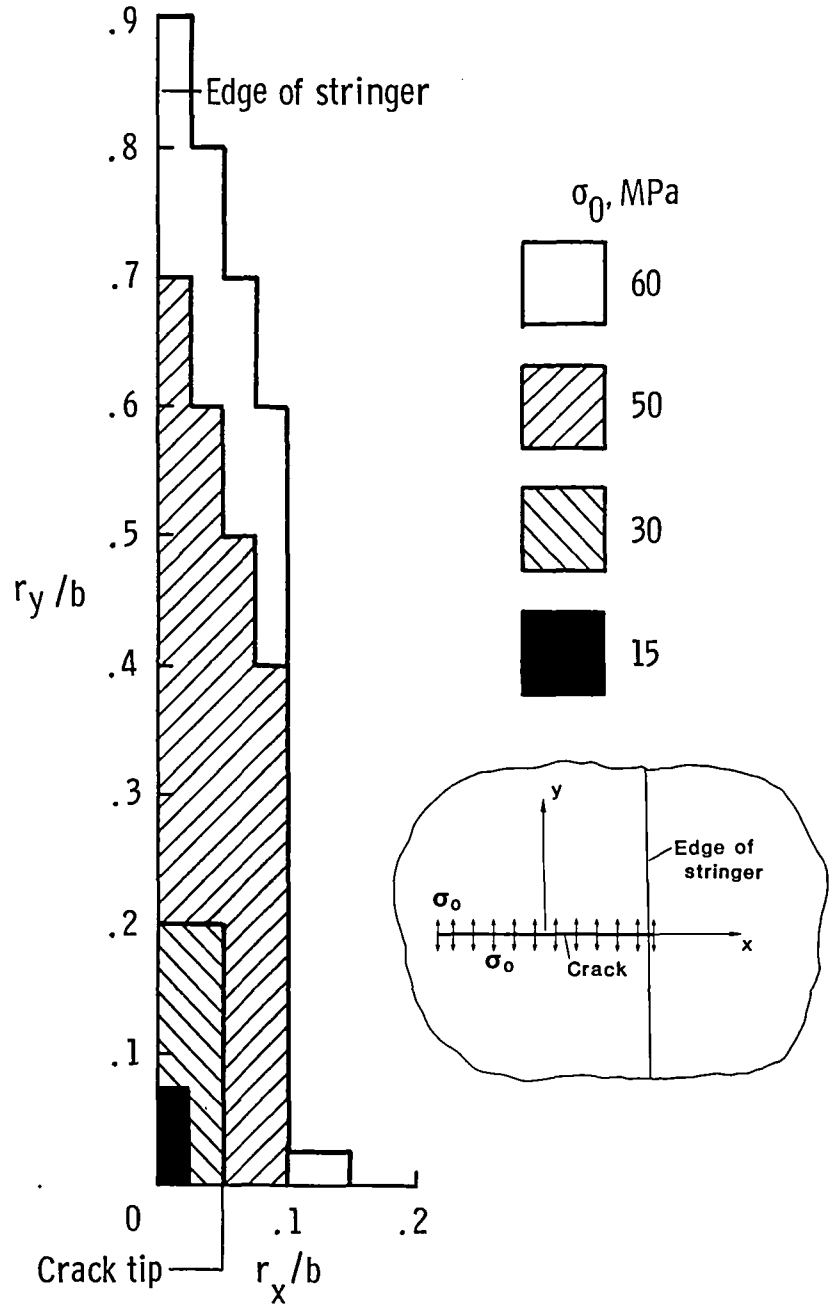

Figure 9. Predicted debond growth in linear adhesive for $a/b = 1.05$.

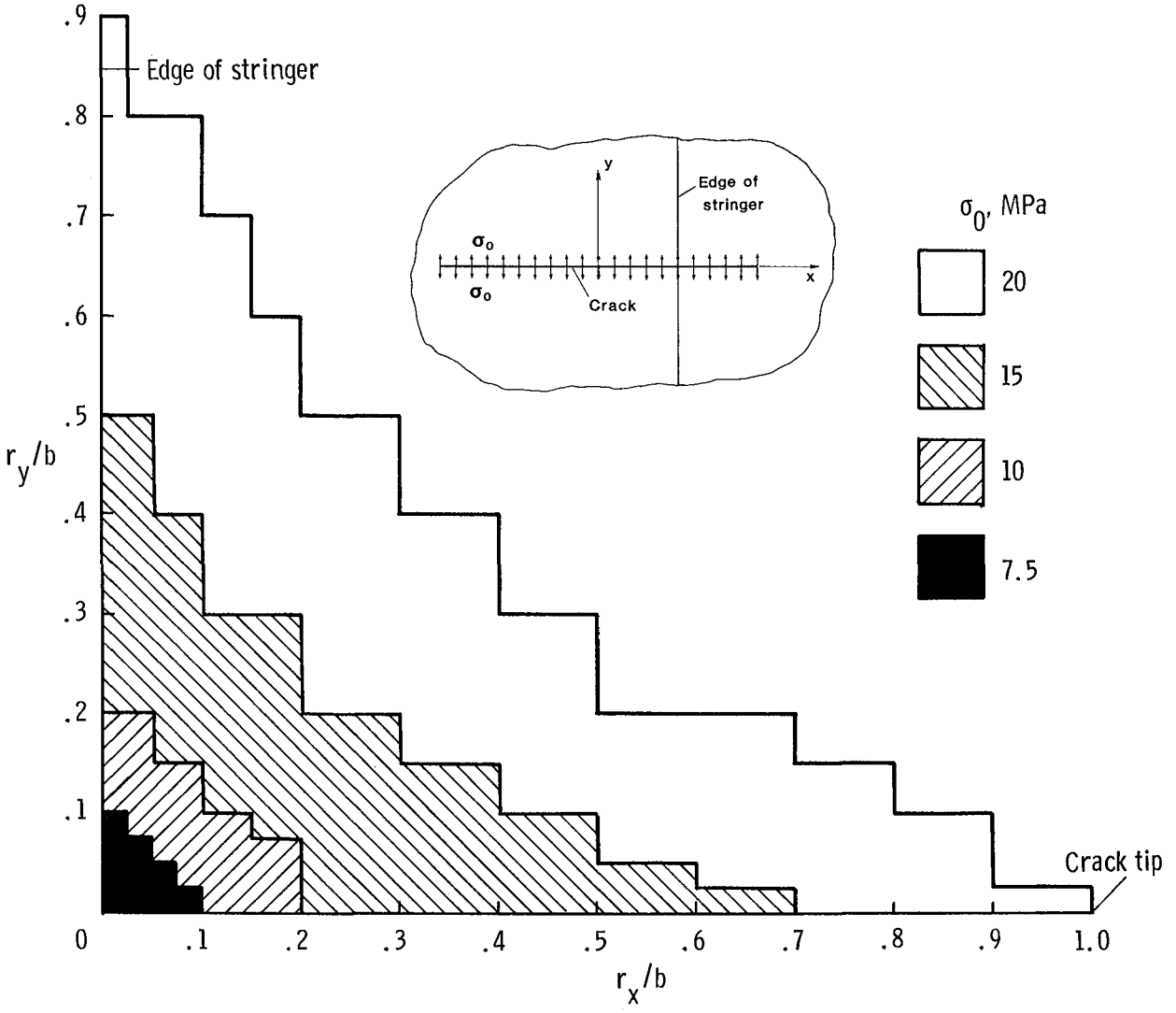

Figure 10. Predicted debond growth in linear adhesive for $a/b = 2.0$.

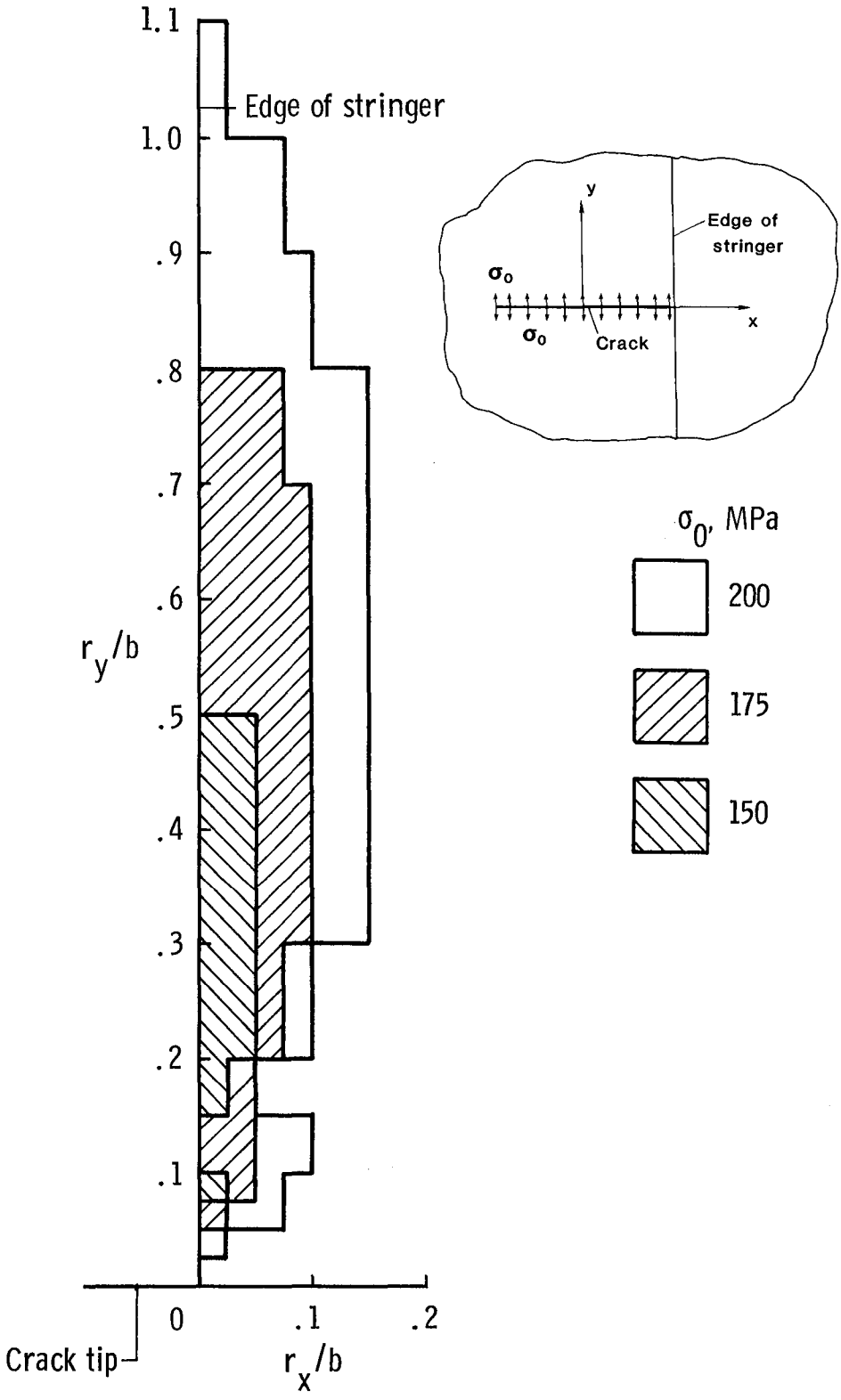

Figure 11. Predicted debond growth in nonlinear adhesive for $a/b = 0.95$.

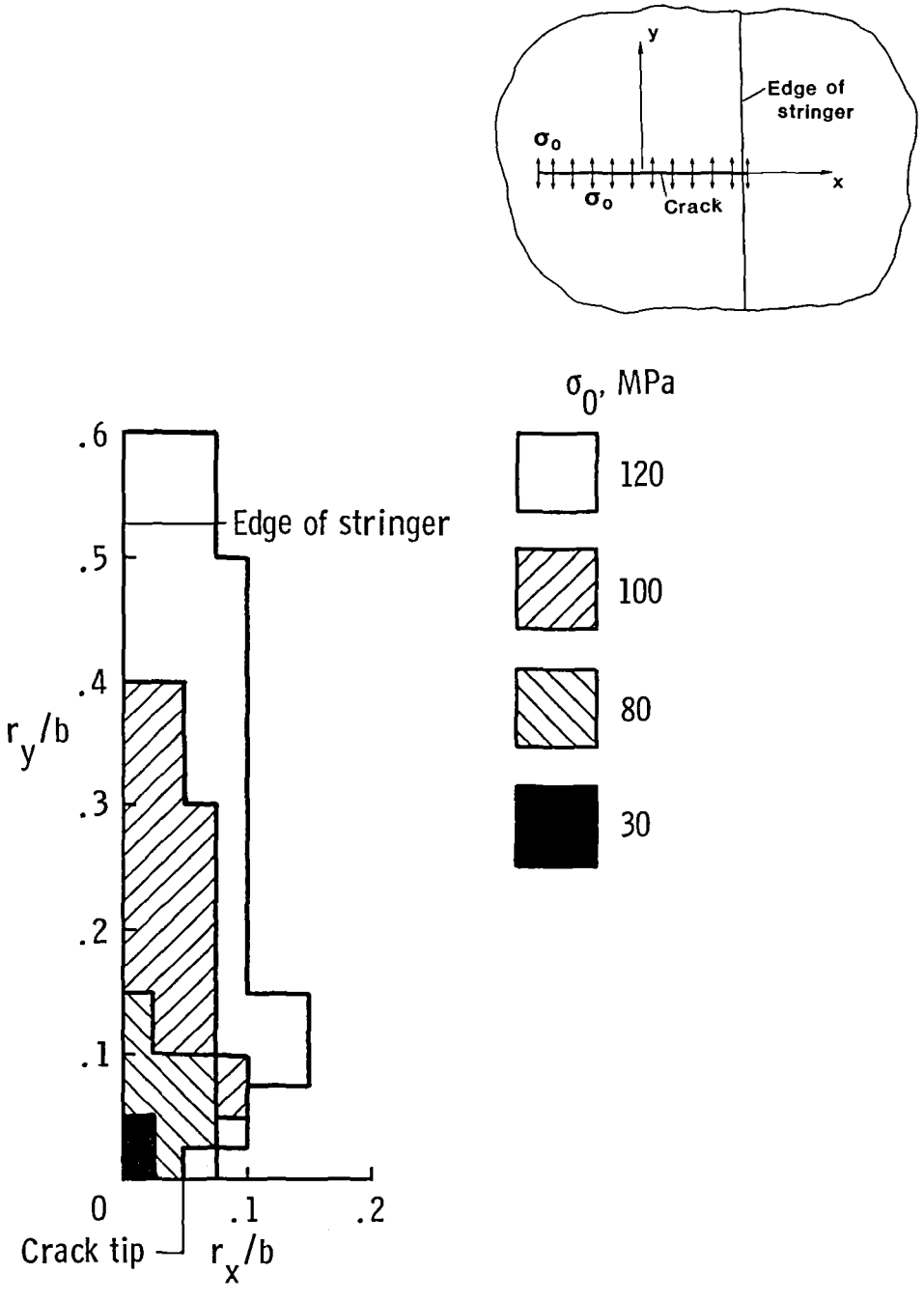

Figure 12. Predicted debond growth in nonlinear adhesive for $a/b = 1.05$.

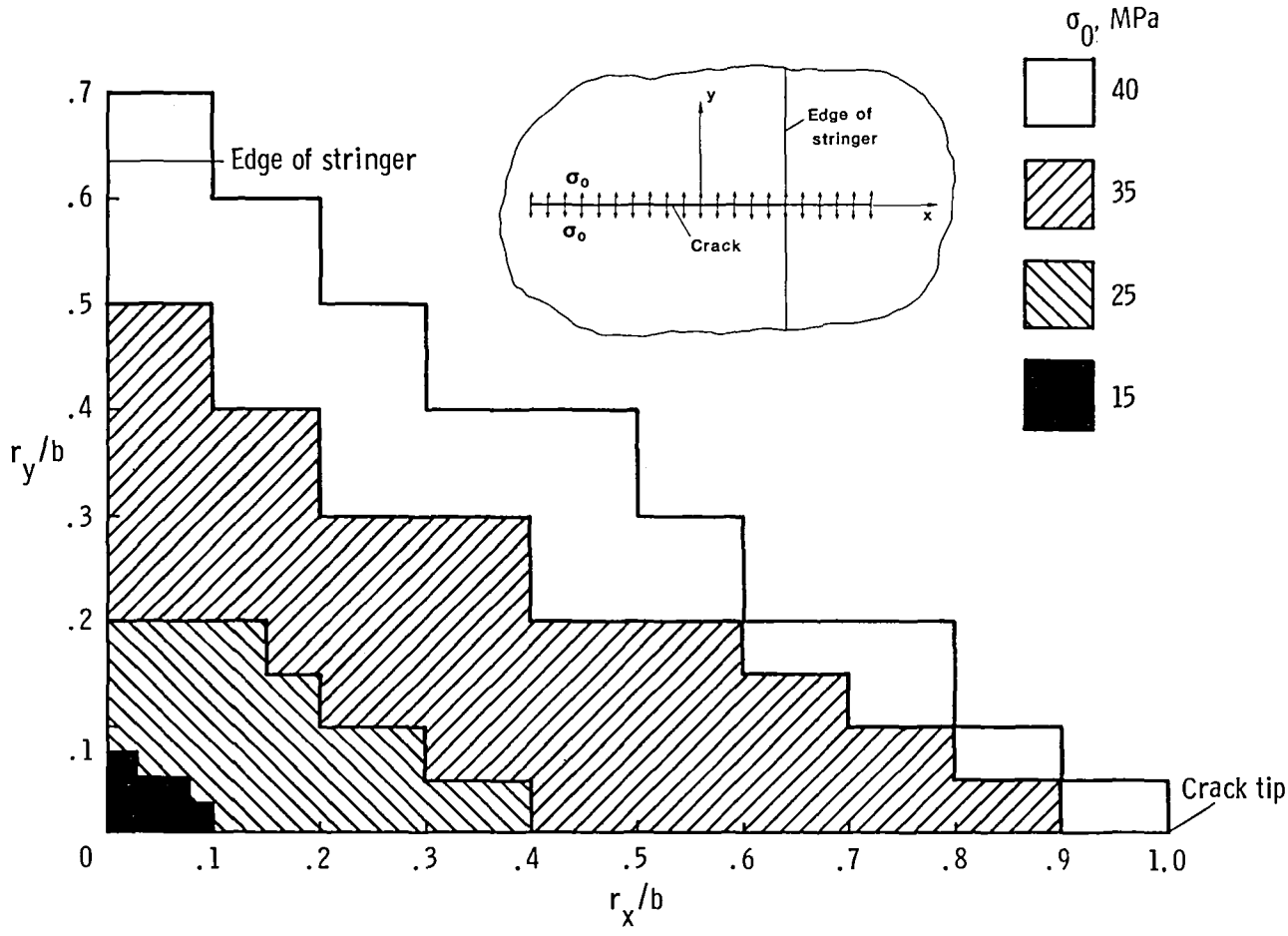

Figure 13. Predicted debond growth in nonlinear adhesive for $a/b = 2.0$.

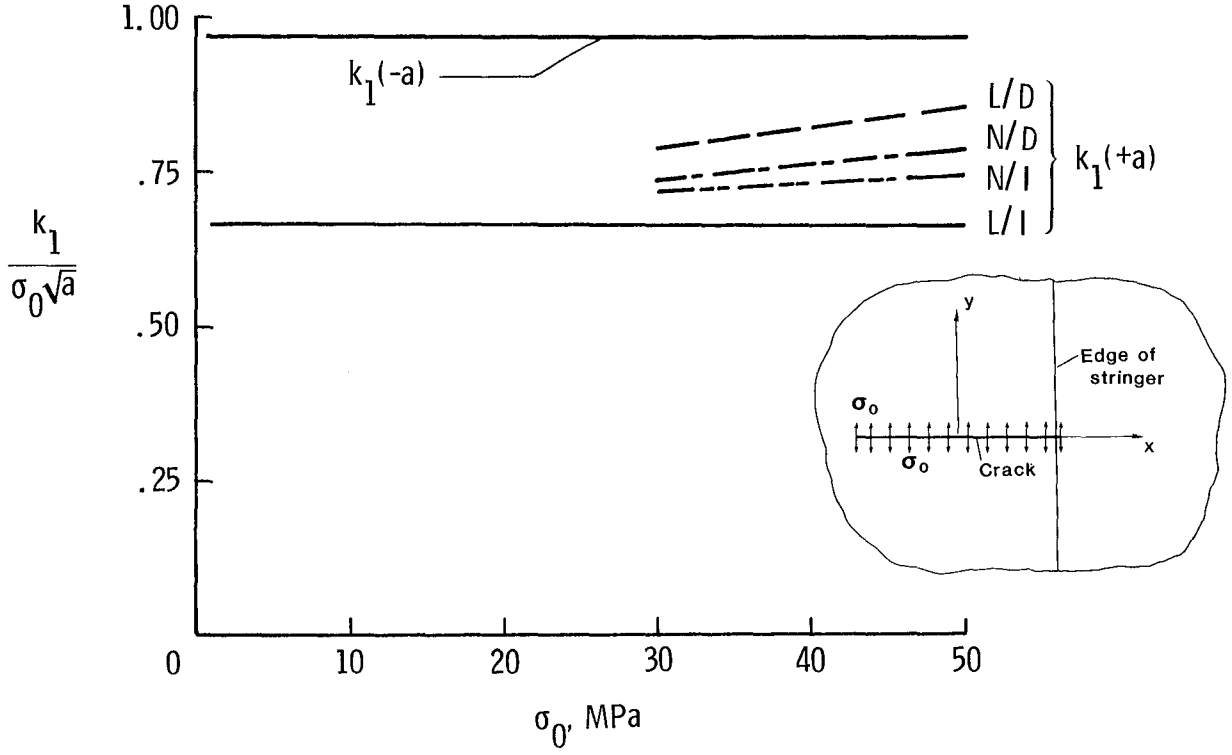

Figure 14. Normalized stress-intensity factors for $a/b = 1.05$.

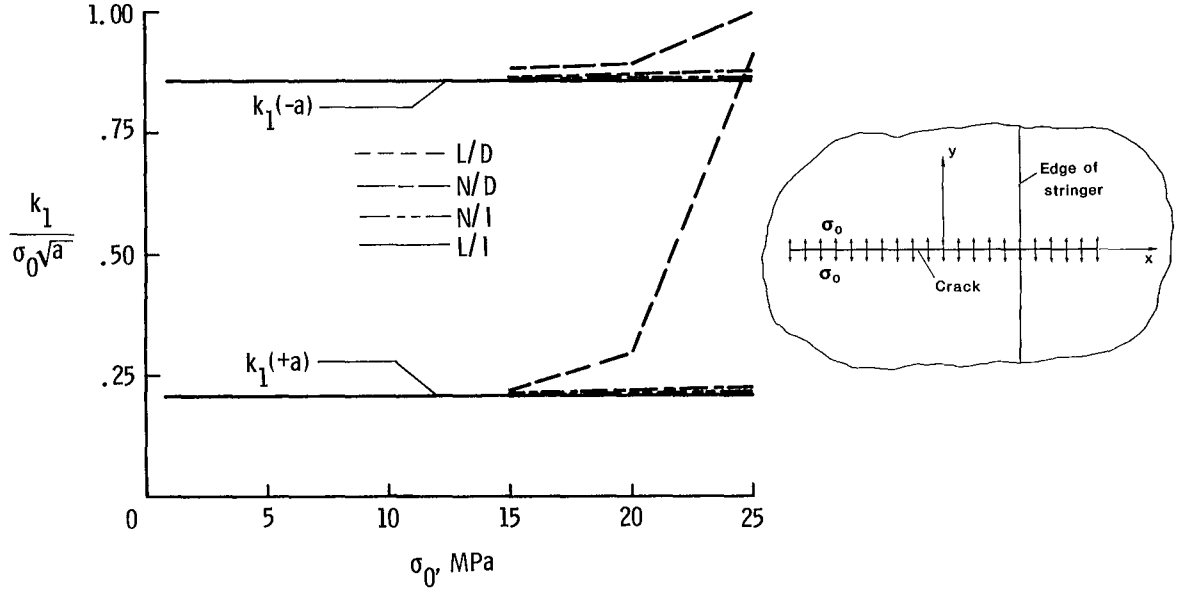

Figure 15. Normalized stress-intensity factors for $a/b = 2.0$.

1. Report No.	2. Government Accession No.	3. Recipient's Catalog No.
NASA TM-87598		

4. Title and Subtitle	5. Report Date
Effect of Debond Growth on Stress-Intensity Factors in a Cracked Orthotropic Sheet Stiffened by a Semi-Infinite Orthotropic Sheet	January 1986
	6. Performing Organization Code: 506-53-23-05
7. Author(s): C. A. Bigelow	8. Performing Organization Report No.: L-16027
9. Performing Organization Name and Address: NASA Langley Research Center, Hampton, VA 23665-5225	10. Work Unit No.
	11. Contract or Grant No.
12. Sponsoring Agency Name and Address: National Aeronautics and Space Administration, Washington, DC 20546-0001	13. Type of Report and Period Covered: Technical Memorandum
	14. Sponsoring Agency Code

15. Supplementary Notes

16. Abstract

Stress-intensity factors are determined for a cracked infinite sheet adhesively bonded to a stringer, and debonding of the adhesive layer is predicted. The stringer is modeled as a semi-infinite sheet. Adhesive nonlinearity is also included. Both the sheet and stringer are treated as homogeneous, orthotropic materials. A set of integral equations is formulated and solved to obtain the adhesive shear stresses and crack-tip stress-intensity factors. Adhesive debonding is predicted using a rupture criterion based on the combined adhesive stresses. When the crack is not under the stringer, the debond extends along the edge of the stringer. When the crack tip is beneath the stringer, the debond grows to the end of the crack, then along the edge of the stringer. Stress levels required for debond initiation decrease as the crack tip is moved beneath the stringer. With a nonlinear adhesive, the debond initiates at higher applied stress levels than in linear adhesive cases. Compared with the linear adhesive solution, modeling a nonlinear adhesive causes the stress-intensity factor to increase when the bond is assumed to remain intact but causes the stress-intensity factor to decrease when debonding is included.

17. Key Words (Suggested by Authors(s))
Composite materials
Adhesive nonlinearity
Integral equations
Stringer panel
Debond prediction

18. Distribution Statement
Unclassified—Unlimited

Subject Category 39

19. Security Classif.(of this report)	20. Security Classif.(of this page)	21. No. of Pages	22. Price
Unclassified	Unclassified	24	A02

For sale by the National Technical Information Service, Springfield, Virginia 22161

NASA-Langley, 1986

National Aeronautics and
Space Administration
Code NIT-4

Washington, D.C.
20546-0001